Overview of HiFi – implicit spectral element code framework for multi-fluid plasma applications.

V. S. Lukin

Space Science Division, Naval Research Laboratory, Washington, DC 20375.

A. H. Glasser, W. Lowrie, E. T. Meier

Plasma Science and Innovation Center,

University of Washington, Seattle, WA 98195

Abstract

An overview of the algorithm and a sampling of plasma applications of the implicit, adaptive high order finite (spectral) element modeling framework, HiFi, is presented. The distinguishing capabilities of the HiFi code include adaptive spectral element spatial representation with flexible geometry, highly parallelizable implicit time advance, and general flux-source form of the partial differential equations and boundary conditions that can be implemented in its framework. Early algorithm development and extensive verification studies of the two-dimensional version of the code, known as SEL, have been previously described [A.H. Glasser & X.Z. Tang, Comp. Phys. Comm., 164 (2004); V.S. Lukin, Ph.D. thesis, Princeton University (2008)]. Here, substantial algorithmic improvements and extensions are presented together with examples of recent two- and three- dimensional applications of the HiFi framework. These include a Cartesian two-dimensional incompressible magnetohydrodynamic simulation of low dissipation magnetic reconnection in a large system, a two-dimensional axisymmetric simulation of self-similar compression of a magnetic plasma confinement configuration, and a three-dimensional Hall MHD simulation of spheromak tilting and relaxation. The ongoing and planned efforts to further improve and expand the capabilities of the HiFi modeling framework are discussed.

I. INTRODUCTION

In computational physics community, there is a large number of existing modeling codes and ongoing development efforts aimed at efficiently and accurately solving some particular set of partial differential equations (PDEs) on two-dimensional (2D) or three-dimensional (3D) grids. Often, such codes are developed with the goal of solving a particular physical or engineering problem, and therefore also assume a particular geometric domain shape. Fully periodic pseudospectral turbulence codes (e.g. Refs. [1, 2]) and toroidally periodic tokamak modeling codes (e.g. Ref. [3]) are prime examples of such development efforts. While being generally effective in solving the problems they were designed for, such codes are difficult or impossible to adapt to model closely-related but geometrically different systems. Similarly, knowledge of the software and significant additional code development effort is usually necessary to modify the system of PDEs under investigation.

On the other hand, there are industry-supported user-friendly software packages for solving general classes of PDE systems on general and complex geometric domains (e.g. COMSOL Multiphysics[4]). However, these packages are either proprietary and unavailable to the research community, or extremely inefficient in solving large problems on modern massively parallel computing systems.

As the demand for computational modeling to simulate existing and planned scientific experiments, and the need to help understand fundamental physics of complex dynamical systems grows, the void between the two types of modeling codes described above is becoming more and more apparent. In this manuscript, we describe the two- and three-dimensional modeling framework called HiFi, which attempts to partially fill this void for a large class of PDEs that can be written in the so-called flux-source form:

$$\frac{\partial Q}{\partial t} + \nabla \cdot \vec{F} = S, \tag{1}$$

where Q, $\vec{F}$, and S are functions of time, space, and the primitive dependent variables, as described below. Most, if not all, fluid plasma models can be cast in this form. (We note that early algorithm development of the 2D version of the HiFi framework, also known as SEL, has been described previously by Glasser & Tang (2004)[5].)

In HiFi, spectral element spatial discretization[6, 7] is used and Eq. (1) is solved in the

weak Galerkin form. The HiFi framework makes use of implicit time-advance, and is therefore most beneficial for problems where dynamical time-scales of interest are much longer than the time it would take the fastest wave to cross the smallest spatial scale being modeled. We use the publicly available PETSc library[8] to solve the large linear systems that arise during the implicit time-advance. This library is continuously supported and updated, and allows easy access to other externally developed direct and iterative linear solvers. All the main features of the code are available both in 2D and 3D versions. The description presented below will assume 3D spatial representation; and, unless noted otherwise, it is implied that the same feature is available in the 2D version. Extensive verification studies of the 2D version of the code have been conducted by Lukin [9] and later continued by Meier [10]. Verification studies of the 3D version of HiFi have been performed and reported by Lowrie [11].

In Section II, we describe the flux-source form given by Eq. (1) in its most general formulation allowed by HiFi. In Section III, the spectral element spatial discretization and the mapping between the logical space, where the numerical integration is done, and the physical space, in which the PDEs are expressed, is presented. Section IV describes the temporal advance options available in HiFi, as well as the techniques we use to accelerate the parallel solution of large linear systems resulting from the implicit formulation. The boundary condition options available in HiFi are listed in Section V. Additional features and the user interface provided in HiFi are described in Section VI. Results of several recent 2D and 3D applications are presented in Section VII. Summary and future development plans are presented in Section VIII.

II. GENERAL FLUX-SOURCE FORMULATION

Any system of coupled PDEs to be evolved in time by HiFi has to be expressed in the following general flux-source form as some M number of PDEs of M primary dependent variables $\{U^i(\vec{x})\}_{i=1,M}$:

$$\left\{ \frac{\partial Q^k}{\partial t} + \nabla \cdot \vec{F}^k = S^k \right\}_{k=1,M} \tag{2}$$

$$
\begin{aligned}
Q^k &\equiv \sum_{i=1,M} \left[A^{ki}(\vec{x}) + \vec{B}^{ki}(\vec{x}) \cdot \nabla \right] U^i \\
\vec{F}^k &= \vec{F}^k(t, \vec{x}, \{U^i\}_{i=1,M}, \{\nabla_{\vec{x}} U^i\}_{i=1,M}) \\
S^k &= S^k(t, \vec{x}, \{U^i\}_{i=1,M}, \{\nabla_{\vec{x}} U^i\}_{i=1,M}),
\end{aligned}
$$

where A^{ki}, $\vec{B}^{ki}$, $\vec{F}^k$, and S^k are arbitrary differentiable functions of the given variables and $\vec{x} = (x, y, z)$ denotes a point vector in the physical metric space $\mathcal{X}$ in which PDEs are expressed (such as Cartesian, cylindrical, or any other well-defined coordinate system chosen by the user). In order to show how this general form is discretized over any logically cubic domain Ξ, we consider a single PDE of the form of Eq. (2) and drop the superscript k. The extension to any M number of PDEs is straightforward.

In any curvilinear metric space Ξ, such that $\vec{\xi} = (\xi, \eta, \phi)$ are the coordinates of Ξ and $\mathcal{J}(\xi, \eta, \phi) \equiv (\nabla z \cdot \nabla x \times \nabla y)(\nabla \phi \cdot \nabla \xi \times \nabla \eta)^{-1}$ is the Jacobian of the transformation from $\mathcal{X}$ to Ξ, it follows from Eq. (2) that:

$$
\mathcal{J} \frac{\partial Q}{\partial t} + \frac{\partial}{\partial \xi^i} (\mathcal{J} \vec{F} \cdot \nabla \xi^i) = \mathcal{J} S. \tag{3}
$$

(Note, in Eq. (3) and everywhere below we assume the usual Einstein summation convention.) Assume that $x^j = x^j(\vec{\xi})$, for $j = 1, 3$ is known. In order to be able to evaluate Eq. (3), it is necessary to know the coordinate transformation $\nabla \xi^i = (\partial \xi^i / \partial x^j) \nabla x^j$, where expressions $(\partial \xi^i / \partial x^j)$ have to be evaluated in Ξ. We compute the transformation between $(\partial x^j / \partial \xi^i)$ and $(\partial \xi^i / \partial x^j)$ under the assumption that $\mathcal{J}$ is non-singular at any location in Ξ where Eq. (3) is to be evaluated.

Having the coordinate transformations at hand, the rest of the computations are done in the Ξ metric space. We call Ξ the logical space, as the computational domain in Ξ is a cube $(\xi, \eta, \phi) \in ([0, 1] \times [0, 1] \times [0, 1])$ with grid distributed uniformly in ξ, η and ϕ. A mappings $(\mathcal{M} : \Xi \rightarrow \mathcal{X})$ then allows the computational domain in the physical space to have an arbitrary shape and curvature of the grid, as long as its topology can be reproduced by identifying corresponding edges of a structured cube grid.

III. SPATIAL DISCRETIZATION

The computational domain in HiFi is spatially discretized using the method of spectral/(hp) elements. (For in-depth discussion on numerical properties of spectral element discretizations see, for example, Karniadakis & Sherwin (1999)[6] and Deville, Fischer, and Mund (2002)[7] and references therein.) Spectral element (or similarly high order finite element) representation combines the flexibility of an adaptable grid that can be shaped to fit any given physical domain, parallelization by domain decomposition, and the exponential spatial convergence, low artificial wave dispersion and dissipation of purely spectral codes. Its basic premise is to have a relatively coarse grid of elements with separate high order polynomial expansions within each element. Thus, each basis function of the overall expansion is identically zero in all but one or at most several neighboring elements. The exact set of basis functions and their coupling across the element boundaries can vary. For example, among the codes presently employed or being developed in the MagnetoHydro-Dynamics (MHD) community, M3D-C1 code[12] uses a set of C^1-continuous finite elements which are constrained to be differentiable as well continuous across the element boundaries, while NIMROD code[3] uses a set of C^0-continuous finite elements which only guarantee the continuity of the solution, but not of its gradients across the element boundaries.

The set of basis functions presently implemented in HiFi is the C^0-continuous set of spectral elements $\{\Lambda^i\}$ given by Jacobi polynomials. (See Figure 1), where all but the linear basis functions identically vanish at the element boundaries. The linear basis functions are the only ones that provide the continuity of the solution and the coupling between the elements in each direction. Representation in ξ, η and ϕ directions of the logical grid described above is done separately with the complete basis of 3D functions formed by the set of non-zero Cartesian products of three unidirectional basis functions $\alpha^n(\xi,\eta,\phi) = \Lambda^i(\xi)\Lambda^j(\eta)\Lambda^k(\phi)$.

Any physical dependent variable $U(t,\vec{x}(\vec{\xi}))$ is expanded in $\alpha^i(\vec{\xi})$ and time-dependent amplitudes $u_i(t)$:

$$U(t,\vec{x}) = u_i(t)\alpha^i(\vec{\xi}) \tag{4}$$

$$U_{x^k}(t,\vec{x}) = u_i(t)\frac{\partial\alpha^i}{\partial\xi^l}\frac{\partial\xi^l}{\partial x^k}. \tag{5}$$

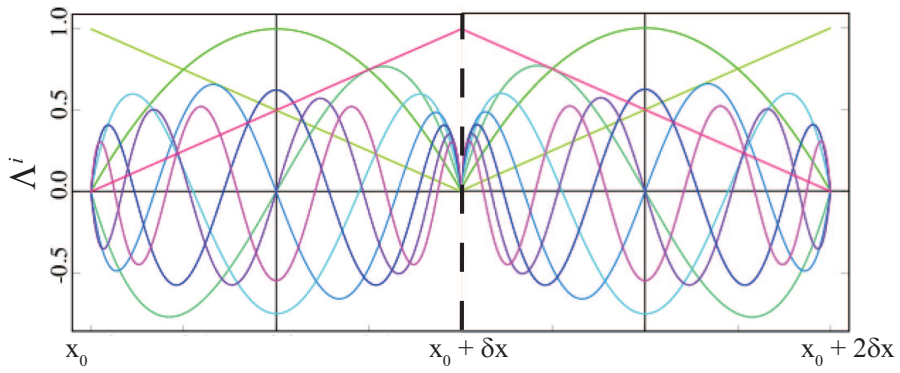

FIG. 1: A one-dimensional illustration of spectral element basis functions Λ^i used in HiFi. Shown are two neighboring cells with Jacobi polynomial $\{\Lambda^i\}_{i:0,n_p=8}$ basis functions in each cell: $\Lambda^0 = (1-\bar{x})/2$, $\Lambda^{n_p} = (1+\bar{x})/2$, and $\Lambda^i = (1-\bar{x}^2)P_i^{(1,1)}(\bar{x})$, for $i = 1, n_p - 1$. In these definitions, $\bar{x} \in [-1, 1]$ is renormalized from $x \in [x_0 + n\delta x, x_0 + (n+1)\delta x]$. Note that Λ^{n_p} from a cell on the left is joined with Λ^0 of the cell on the right to form a single basis function to insure continuity, while all other basis functions vanish at $x = x_0 + \delta x$.

We note that $x^k(\vec{\xi})$ can be represented similarly as:

$$x^k(\vec{\xi}) = x_i^k \alpha^i(\vec{\xi}). \tag{6}$$

Thus, if at some time t_0 during a simulation it becomes desirable to move the calculation from a grid in the physical space represented by a mapping $(\mathcal{M} : \Xi \to \mathcal{X})$ to a new grid represented by a new mapping $(\mathcal{M}' = \mathcal{L}\mathcal{M} : \Xi \to \mathcal{X})$, where $\mathcal{L}$ is some mapping $(\mathcal{L} : \Xi \to \Xi)$; $U(t_0, \vec{x})$ and $\vec{x}(\vec{\xi})$ would all be remapped in the same manner.

Observe that Eq. (3) can be rewritten as:

$$\mathcal{J}\frac{\partial Q}{\partial t} + \frac{\partial}{\partial \xi^j}\left[F_{x^i}\mathcal{J}\frac{\partial \xi^j}{\partial x^i}\right] = \mathcal{J}S, \tag{7}$$

where $\{F_{x^i} \equiv \vec{F} \cdot \nabla x^i\}_{i=1,3}$ are the components of the flux of U in the physical space $\mathcal{X}$. Reformulating Eq. (7) in the weak form, we have:

$$\begin{aligned}
\left\{\mathbb{M}^{ji}\dot{u}_i \right. &\equiv \int \mathcal{J}dV\alpha^j\left(A\alpha^i + \vec{B}\cdot\nabla\alpha^i\right)\dot{u}_i \\
&= \int \mathcal{J}dV\left[S\alpha^j + F_{x^i}\left(\frac{\partial \xi^k}{\partial x^i}\frac{\partial \alpha^j}{\partial \xi^k}\right)\right] + boundary \\
&\equiv \left. r^j\left(t, \{u_k\}_{k=1,N}\right)\right\}_{j=1,N},
\end{aligned} \tag{8}$$

where $dV \equiv d\xi\ d\eta\ d\phi$ and N is the size of the spectral element basis and therefore is the number of degrees of freedom in this time-dependent vector equation. (For a system of M PDEs on a logical grid with n_x, n_y, n_z elements in x-, y-, and z-directions, respectively, and polynomial basis expansion up to the n_p-th order, the total number of degrees of freedom is $N = M * n_x * n_y * n_z * n_p^3$.)

With the derivation above, we have shown how the generalized flux-source formulation allows for advancing spatially discretized set of PDEs in an arbitrary logically cubic domain, while the physical equations can be specified in an unrelated coordinate system most convenient for one's particular application. We note that fluxes F_x, F_y, F_z and source S, together with $A(\vec{x})$ and $\vec{B}(\vec{x})$, completely specify the PDEs for any given problem, and the coordinate transformation map $\vec{x}(\vec{\xi})$ specifies its geometry; with these as input, Eq. (8) contains all necessary information about HiFi's spatial discretization to have the solution advanced in time. Such separation of physics, geometry and solution algorithm is the key to the structural organization of the HiFi framework.

IV. ADAPTIVE TEMPORAL ADVANCE ALGORITHM

The implicit temporal advance in HiFi is accomplished by the Newton-Krylov iterative method[5, 9]. However, like the rest of the framework, the time-advance module of HiFi is designed to be easily modifiable for any number of particular time-discretization schemes. The principle time-dependent equation to be solved is Eq. (8), which can be written as a vector equation:

$$\mathbb{M}\dot{\mathbf{u}} = \mathbf{r}(t, \mathbf{u}). \tag{9}$$

Presently, two well known algorithms are implemented to solve Eq. (9): the Θ-scheme, with an adjustable time-centering parameter θ; and a 2^{nd} order backward differencing formula (BDF2)[13]. Below, we briefly outline each of the time-discretization schemes. We then describe the implementation of the Newton-Krylov iterative advance itself and the adaptive time-stepping algorithm.

A. Θ-scheme:

Equation (9) is discretized as

$$\mathbb{M}\left(\frac{\mathbf{u}^{n+1}-\mathbf{u}^{n}}{h}\right)=\theta\mathbf{r}\left(t^{n+1},\mathbf{u}^{n+1}\right)+(1-\theta)\mathbf{r}\left(t^{n},\mathbf{u}^{n}\right), \tag{10}$$

where $h \equiv \delta t^{n+1} = t^{n+1} - t^{n}$ is the size of the $(n+1)$-st time-step. With $\theta = .5$, the Θ-scheme is known as the Crank-Nicholson method and is an implicit second order non-dissipative time-discretization method. All of the application examples presented in Section VII advanced PDEs describing appropriate physical systems with the Crank-Nicholson method. However, with θ as a run-time input parameter, both $\theta = 0$ explicit and $\theta = 1$ first order dissipative implicit methods can also be used for purposes of testing novel PDE implementations.

In order to solve Eq. (10) for $\mathbf{u}^{n+1}$ by Newton's iteration, an initial guess is set to $\mathbf{u}_0^{n+1} \equiv \mathbf{u}^{n}$, the change in the solution being sought is denoted by $\delta\mathbf{u}_i \equiv \mathbf{u}_{i+1}^{n+1} - \mathbf{u}_i^{n+1}$, the residual $\mathbf{R}$ is defined as

$$\begin{aligned}\mathbf{R}\left(\mathbf{u}_i^{n+1}\right) &\equiv \mathbb{M}\delta\mathbf{u}_i \\ &- h\left[\theta\mathbf{r}\left(t^{n+1},\mathbf{u}_i^{n+1}\right)+(1-\theta)\mathbf{r}\left(t^{n},\mathbf{u}^{n}\right)\right],\end{aligned} \tag{11}$$

and the Jacobian of the iteration is defined as

$$\mathbb{J}^{ij} \equiv \mathbb{M}^{ij} - h\theta\left\{\frac{\partial r^{i}}{\partial u_j}\right\}_{t=t^{n+1},\mathbf{u}=\mathbf{u}^{n}}. \tag{12}$$

B. BDF2 scheme:

Equation (9) is discretized as

$$\mathbb{M}\left(\frac{\mathbf{u}^{n+1}-a\mathbf{u}^{n}+b\mathbf{u}^{n-1}}{h}\right)=\mathbf{r}^{n+1}, \tag{13}$$

where

$$a \equiv \frac{\left(\delta t^{n}+\delta t^{n+1}\right)^{2}}{\delta t^{n}\left(\delta t^{n}+2\delta t^{n+1}\right)},$$

$$b \equiv \frac{\left(\delta t^{n+1}\right)^2}{\delta t^n \left(\delta t^n + 2\delta t^{n+1}\right)},$$

$$h \equiv \frac{\delta t^{n+1} \left(\delta t^n + \delta t^{n+1}\right)}{\left(\delta t^n + 2\delta t^{n+1}\right)},$$

$\delta t^n = t^n - t^{n-1}$, and $\delta t^{n+1} = t^{n+1} - t^n$. Here, an initial guess is set to $\mathbf{u}_0^{n+1} \equiv a\mathbf{u}^n - b\mathbf{u}^{n-1}$, change in the solution is again $\delta \mathbf{u}_i \equiv \mathbf{u}_{i+1}^{n+1} - \mathbf{u}_i^{n+1}$, the residual is defined as

$$\mathbf{R}\left(\mathbf{u}_i^{n+1}\right) \equiv \mathbb{M}\delta\mathbf{u}_i - h\mathbf{r}\left(t^{n+1}, \mathbf{u}_i^{n+1}\right), \tag{14}$$

and the Jacobian of the iteration is

$$\mathbb{J}^{ij} \equiv \mathbb{M}^{ij} - h\left\{\frac{\partial r^i}{\partial u_j}\right\}_{t=t^{n+1}, \mathbf{u}=\mathbf{u}^n}. \tag{15}$$

Like Crank-Nicholson, BDF2 is also a second order time-discretization method. However, straightforward analysis of Eq. (13) demonstrates that BDF2 damps high time-frequency modes of the solution, thus providing numerical dissipation in the algorithm. When using the BDF2 scheme, we resolve the issue of the first time-step by making the first time-step with the Θ-scheme, and then taking the initial condition and the first time-step as the $(n-1)$-st and the n-th values of $\mathbf{u}$, respectively. We also note that Eqs. (13)-(15) explicitly allow for $\delta t^{n+1} \neq \delta t^n$, which is necessary to have an adaptive time-stepping algorithm.

Using either of the time-discretization schemes described above, time advance is accomplished by iterating on

$$\begin{aligned} \mathbf{R}_i + \mathbb{J}\delta\mathbf{u}_i = 0 \;&\rightarrow\; \delta\mathbf{u}_i = -\mathbb{J}^{-1}\mathbf{R}_i \\ &\rightarrow\; \mathbf{u}_{i+1}^{n+1} = \mathbf{u}_i^{n+1} + \delta\mathbf{u}_i \\ i \;&\Rightarrow\; i+1 \end{aligned} \tag{16}$$

until the condition $\mathfrak{N}(\mathbf{R}_i) \leq n_{tol}$ is satisfied, where $\mathfrak{N}$ is the $\mathbb{L}^2$ norm of $\mathbf{R}_i$ normalized to $\mathbf{R}_0$ and n_{tol} is a run-time input parameter determining the tolerance of the Newton iteration convergence. Once the Newton iteration has converged, the solution vector is advanced by setting $\mathbf{u}^{n+1} = \mathbf{u}_{i+1}^{n+1}$. An advanced non-linear Newton solver available through PETSc, *SNESSolve*[8], is used in the current HiFi implementation to complete the above cycle.

The Newton iteration procedure includes a non-trivial step of solving the matrix $\mathbb{J}$, which is an $N \times N$ sparse matrix, where N is the total number of degrees of freedom. In fact, $\mathbb{J}$ describes the exact coupling between each of the degrees of freedom at time $t = t^n$. However, due to the C^0 nature of the basis functions employed in HiFi, only "skeletons" representing the linear basis functions (linear in at least one direction) within each cell are coupled to each other across the cell boundaries. The so-called static condensation procedure[6] separates the skeletons from the interiors of the cells and uses separate local solves for each of the cell's interiors[5]. By doing so, static condensation both reduces the size of the global matrix to be solved by a factor of n_p and significantly improves the parallel efficiency of the code. We note that in order to enable the static condensation algorithm, the matrix $\{\partial r^i/\partial u_j\}$ involved in calculating $\mathbb{J}$ in both Eq. (12) and Eq. (15) has to be calculated explicitly by taking derivatives of Eq. (8) with respect to all degrees of freedom in the system. This is accomplished by specifying the analytical derivatives of the fluxes F_{x^i} and sources S with respect to the evolved physical variables U and their gradient components U_{x^i}. Though somewhat labor-intensive in coding, this method allows for much greater accuracy of the time-advance algorithm.

An additional method of preconditioning the HiFi linear system is presently under development. So-called physics-based preconditioning (PBP), originally developed by Luis Chacòn in the context of a finite volume spatial discretization[14], is designed to achieve near-perfect weak scalability in solving linear systems resulting from implicit advance of discretized MHD systems over tens of thousands of processors and beyond.

The remaining global matrix is solved in parallel using the PETSc libraries[8] with the linear solvers available and appropriate for any given problem. Choice of any particular solver, such as direct LU factorization or the flexible Generalized Minimal Residual (fGMRES) method, is made at run-time and requires no modifications to the code. Local solves are accomplished with LAPACK routines.

We now return to Equation (16) and consider what happens if a time step δt^{n+1} taken in Eq. (10) for Θ-scheme or in Eq. (13) for BDF2 is either unnecessarily small, so that Newton iterations converge *too quickly*, or so large that *too many* iterations are necessary for convergence. Run time input parameters $newt_{max}$ and $newt_{min}$ define those limits for each particular simulation run. The automatic adaptivity of the time-step is accomplished by decreasing δt^{n+1} by some fraction $f_{decr} < 1$ and recalculating the Jacobian whenever Eq. (16)

has not converged after $newt_{max}$ Newton iterations. Conversely, δt^{n+1} is set to $\delta t^{n+1} = f_{incr}\delta t^n$, $f_{incr} > 1$, whenever the Newton iterations of the previous time-step converged in less than $newt_{min}$ number of iterations. For iterative linear solvers such as fGMRES, the number of fGMRES iterations can be an additional factor in determining whether or not to increase/decrease the time step. This simple algorithm has proven to be very robust and useful in modeling systems that have both long periods of slow and/or linear evolution and bursts of activity with very short non-linear dynamical time-scales[9].

Additional performance gain has been achieved by re-evaluating the Jacobian $\mathbb{J}$ only during those time-steps when the number of Newton iterations it_N taken during the previous time-step was equal or greater than $newt_{max}$. However, if $newt_{max} > it_N \geq newt_{min}$, the Jacobian matrix used during the previous time-step is re-used without being re-evaluated. While allowing for significant gain in performance, particularly during quasi-linear periods of evolution in any number of non-linear simulations, this technique does not lead to any deterioration in the accuracy of the computation.

V. FORMULATION OF BOUNDARY CONDITIONS

As indicated in Eq. (8), formulation of boundary conditions in HiFi is integrated into the overall flux-source form. All quantities are advanced in time on the boundary and in the interior of the domain in a single time-step by solving the primary system of PDEs in the interior together with a separate system of PDEs describing the boundary conditions on the boundary nodes. Two classes of general boundary condition (BC) forms, as well some special cases, are available in HiFi.

We call one of the BC classes – the explicit local BC form, where the solution on the boundary must satisfy a general non-linear time-dependent equation of the form

$$\left\{ \left[A^{ki} \frac{\partial U^i}{\partial t} + \vec{B}^{ki} \cdot \nabla \left(\frac{\partial U^i}{\partial t} \right) \right] = S^k \right\}_{k=1,M} \tag{17}$$

$$S^k = S^k \left(t, \hat{n}, \vec{x}, \{U^i, \nabla_{\vec{x}} U^i, \nabla_{\vec{x}\vec{x}} U^i\}_{i=1,M} \right)$$

where $A^{ki} = A^{ki}(\hat{n}, \vec{x})$, $\vec{B}^{ki} = \vec{B}^{ki}(\hat{n}, \vec{x})$, and S^k are arbitrary differentiable functions of the given variables and $\hat{n}$ denotes an outward unit vector normal to the boundary of the domain.

The other BC class – the flux BC form, allows users to specify the desired normal flux

$F_n \equiv \vec{F} \cdot \hat{n}$ of a particular primary dependent variable through the boundary of the domain. Once again,

$$F_n = F_n \left(t, \hat{n}, \vec{x}, \{U^i, \nabla_{\vec{x}} U^i, \nabla_{\vec{x}\vec{x}} U^i\}_{i=1,M} \right) \tag{18}$$

can be an arbitrary differentiable function of the given variables.

Two special boundary condition options are also available: (1) periodic BC's in any or all directions can be imposed on the full system, or on specific dependent variables; (2) cylindrical BC can be imposed on the system, such that for any $\eta_0 \in [0, 1]$, all points $(\xi, \eta, \phi) \in (\xi, \eta_0, 0)$ in the 3D logical space are identified together. (In the 2D implementation, there is an equivalent polar BC option, where all points $(\xi, \eta) \in (0, \eta)$ in the 2D logical space are identified together.)

VI. USER INTERFACE AND ADDITIONAL FEATURES

Making use of the generic implementation of the primary PDE system, boundary conditions, and the physical domain shape – the HiFi user interface consists of a standardized set of subroutines collected into a *physics* template file. Within the template file, the user has the freedom

1. to specify the functional forms that would uniquely determine Eq. (2);

2. to choose the class of boundary conditions separately on each face for each dependent variable and subsequently specify the necessary functional forms to uniquely determine either Eq. (17) or Eq. (18);

3. to specify the initial map between the logical and physical spaces;

4. to specify the initial conditions, as well as the set of user-desired input variables for the problem at hand.

The rest of the HiFi algorithm is separated and compiled into a library, that can be used with any *physics* application file constructed according to the template. We note that as long as the set of specified primary PDEs and boundary conditions has a unique solution, any of the free functions provided in Eqs. (2,17,18) can also be set to zero.

One of the most attractive additional features of the HiFi framework is grid adaptation. There are a number of strategies and approaches that have been attempted in the computational physics community to enable accurate and efficient grid adaptation for solving initial-value problems with multi-scale spatial behavior. They can be generally divided into two groups: adaptive mesh refinement (AMR), where parts of the grid with insufficient resolution are refined by effectively subdividing the existing grid cells[15, 16]; and dynamic Arbitrary-Lagrangian-Eulerian (ALE) techniques[17–19] and/or variational principle based harmonic grid generation[20–22], where an evolving mapping between some logical grid of a fixed size and the physical domain provides the necessary adaptation. Algorithms that combine the two approaches are also being developed[23]. While each of the methods has its advantages and drawbacks in flexibility, accuracy and parallel efficiency, we have chosen to pursue a harmonic grid generation method which appears to be highly accurate, relatively flexible and does not in any way inhibit the parallel efficiency of the HiFi framework. We have collaborated with Liseikin[24] in the development of such grid generation algorithm capable of finding an optimal mapping $\mathcal{M}$ between the logical domain Ξ and given physical domain $\mathcal{X}$. The details of the HiFi adaptive grid implementation and verification studies have been reported by Lukin[9] and will be further described in a follow-up manuscript.

Another useful feature of HiFi is the ability to restart a simulation from a previously generated check-point data file, while either increasing or decreasing the overall resolution of the restarted simulation. Furthermore, such previously generated data may come from a solution of an entirely different set of PDEs with different dependent variables: for example, the user can read in the solution of some anisotropic heat conduction equation to initialize the temperature in a compressible MHD simulation.

We take advantage of the parallel HDF5 libraries[25] for the check-point data input and output (IO). In order to visualize or extract quantitative physically meaningful results from the computed data, the check-point files are additionally post-processed. Parallel post-processing is presently available for the 3D data. HiFi's primary visualization tool, particularly in 3D, is the publicly available VisIt Visualization Tool[26].

VII. SAMPLE PLASMA APPLICATIONS

A number of publications reporting results obtained with various applications of the HiFi framework are already available. HiFi has been used to study idealized physical systems[27, 28], to conduct realistic simulations with validation against experimental data[29, 30], to study numerical properties of the C^0 spectral element spatial discretization[31, 32], and to develop and test new numerical methods, in particular, for accurate formulation of "open" boundary conditions in mixed hyperbolic-parabolic systems of PDEs[33]. Here, we briefly describe several ongoing applications and test verification problems solving different sets of PDEs with the 2D and 3D HiFi versions in order to demonstrate the accuracy and flexibility of the framework.

A. Reduced MHD plasmoid-facilitated magnetic reconnection

One of the simplest 2D systems of PDEs that describe behavior of a magnetized plasma is the visco-resistive reduced (incompressible) MHD system of equations, which is valid in the limit of strongly magnetized collisional plasma. Assuming no initial variation in the out-of-plane $\hat{z}$-component of magnetic field $\mathbf{B}$ and no initial out-of-plane plasma flow $\mathbf{v}$, this system of PDEs can be written in the flux-source form as follows:

$$\frac{\partial \psi}{\partial t} + \nabla \cdot (\psi \hat{z} \times \nabla \phi) = \nu j \tag{19}$$

$$\frac{\partial \omega}{\partial t} + \nabla \cdot [\omega \hat{z} \times \nabla \phi - j \hat{z} \times \nabla \psi - \mu \nabla \omega)] = 0 \tag{20}$$

$$\nabla \cdot [\nabla \psi] = j \tag{21}$$

$$\nabla \cdot [\nabla \phi] = \omega, \tag{22}$$

where ψ is the magnetic flux function with $\mathbf{B} = \hat{z} \times \nabla \psi$, ϕ is the plasma flow stream function with $\mathbf{v} = \hat{z} \times \nabla \phi$, ν is isotropic plasma resistivity and μ is isotropic kinematic viscosity. HiFi implementation of and simulations using Eqs. (19-22) have been reported previously[5, 9]. Here, we present results of a magnetic reconnection simulation similar to those described by Lukin[9], but with lower dissipation parameters ν and μ.

The reduced visco-resistive MHD equations, Eqs. (19-22), are solved in a rectangular box $(x, y) \in [-L_x, L_x] \times [-L_y, L_y]$. Periodic boundary conditions are used in the reconnection

outflow $\hat{x}$-direction, while an "open" boundary is assumed in the inflow $\hat{y}$-direction in order to reduce the effects of the domain boundary on the reconnection layer. Here, we define "open" boundary to have zero tangential flow, zero vorticity and constant and uniform tangential component of magnetic field. Thus, on the y-boundary, $\hat{y}\cdot\nabla\phi = 0$, $\nabla^2\phi = 0$, and $\hat{y}\cdot\nabla\psi = const$ are the enforced BC. Simulations are initialized with a Harris equilibrium[34] with an additional small and localized perturbation: $\psi_0 = \lambda \ln[\cosh(y/\lambda)] + \delta\psi$, $\delta\psi = \epsilon \exp[-x^2/(2\lambda)^2] \exp[-y^2/(\lambda/2)^2]$, where λ is the half-width of the Harris equilibrium and ϵ is the magnitude of the perturbation. Note that the perturbation is localized within the equilibrium current sheet.

In order to model the development of a macroscopic resistive current layer from a local perturbation in a large system, the following simulation parameters are chosen: $\lambda = .5$, $L_x = 48$, $L_y = 4$, $\epsilon = 10^{-4}$ and $\nu = \mu = 10^{-5}$, where the width of the initial Harris equilibrium is taken as the effective unit length. Making use of the symmetries of the initial conditions and those inherent in Eqs. (19-22), simulations are conducted only in the top-right quarter domain and appropriate symmetry BC are applied. No grid adaptation is used in the simulation. However, a smooth mapping $\{\mathcal{M} : (\xi,\eta) \rightarrow (x,y) = (L_x\xi, L_y[\tanh(\alpha\eta - \alpha)/\tanh(\alpha)+1])\}$ between the logical and physical spaces with $\alpha = 2$ provides computational grid that is highly concentrated near $y = 0$, where the thin resistive reconnection layer shown in Figure 2 forms during the simulation.

Figure 2 shows contour plots of (a,b) magnetic flux ψ, (c,d) stream function ϕ and (e,f) current density j from the simulation on the logical grid of size $(n_x, n_y, n_p) = (108, 48, 8)$. Note that panels (a-d) show the full computational domain, while panels (e,f) show a zoom-in into the reconnection region. It is apparent that results both in panels (a,c,e), showing a single highly elongated reconnection region at $t = 1240$, and in panels (b,d,f), showing the reconnection region that continues to elongate and simultaneously splinters into multiple shorter current sheets at $t = 1320$, are very well resolved.

Yet, we have not been able to converge the simulation setup presented here in spatial resolution. Decreasing the resolution causes the reconnection current sheet to splinter earlier, generating multiple magnetic islands and current sheets. On the other hand, increasing the resolution prolongs the single highly elongated current layer reconnection and expansion until some later time, when it eventually succumbs to what appears to be the multiple plasmoid instability described by Loureiro, *et al.*[35]. Thus, the macroscopic behavior of

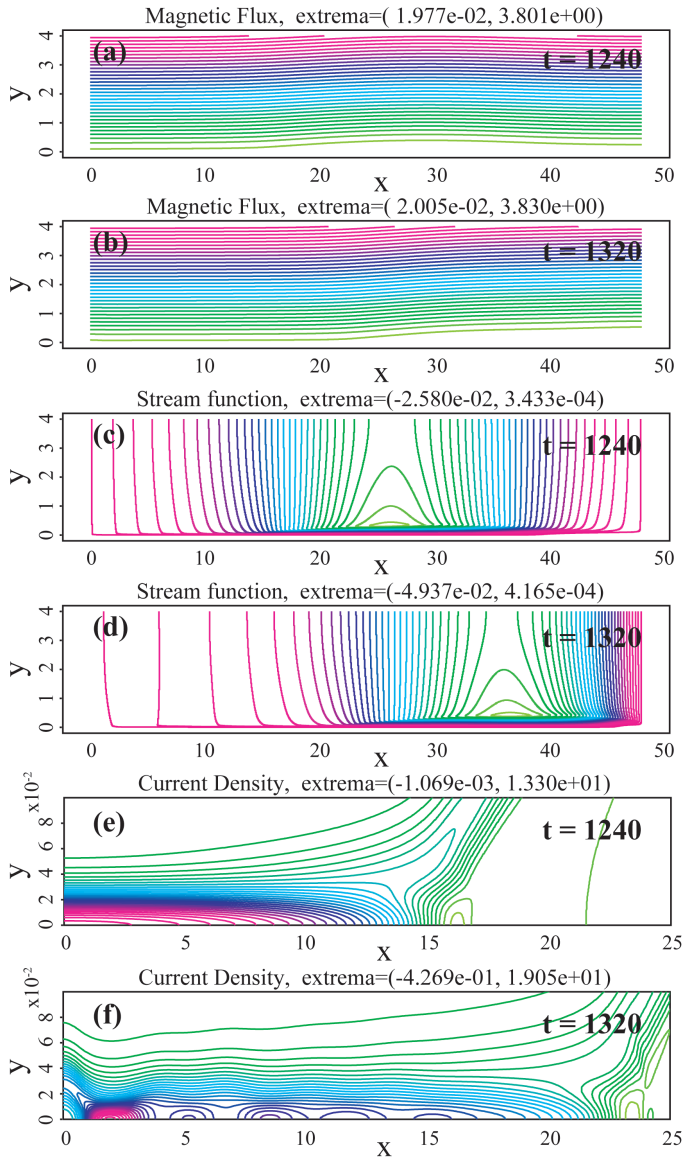

FIG. 2: Contour plots of (a,b) magnetic flux ψ, (c,d) stream function ϕ and (e,f) current density j from a 2D reduced MHD magnetic reconnection simulation. Panels (a-d) show the full computational domain, while panels (e,f) show a zoom-in into the reconnection region. Panels (a,c,e) show a single highly elongated reconnection region at $t = 1240$; while a short time later at $t = 1320$, panels (b,d,f) show the reconnection region that continues to elongate and simultaneously splinters into multiple shorter current sheets. The simulation is conducted with resistivity $\nu = 10^{-5}$ and viscosity $\mu = 10^{-5}$.

this system is critically influenced by the level of background noise, determined here by the spatial resolution. Similar behavior in semi-collisional Hall MHD magnetic reconnection simulations has also been previously observed[9].

We note that in a real physical system some level of background noise is always present and the system size is limited by the curvature of the global magnetic fields. Therefore, we

expect that in strongly magnetized collisional plasmas, for any given degree of collisionality, the length of a macroscopic reconnection region and the characteristic number of plasmoids, if any, on average contained within the reconnection region, are determined by the magnitude of the background noise level relative to the rate of the reconnection region expansion.

B. FRC compression in visco-resistive MHD

Another recent application of the HiFi framework is a 2D model of Magnetized Target Fusion (MTF)[36, 37]. The usual compressible MHD system of PDEs is solved with 6 dependent variables, $(\rho, -A_\phi, p, \rho v_z, \rho v_r, J_\phi)$. The equations in cylindrical r, z coordinates are

$$\frac{\partial \rho}{\partial t} + \nabla \cdot (\rho \mathbf{v} - D\nabla\rho) = 0 \tag{23}$$

$$-\frac{\partial A_\phi}{\partial t} = v_r B_z - v_z B_r + \eta J_\phi \tag{24}$$

$$\frac{3}{2}\frac{\partial p}{\partial t} + \nabla \cdot \left(\frac{5}{2} p\mathbf{v} - \kappa \cdot \nabla T\right) = \eta J_\phi^2 + \pi : \nabla \mathbf{v} \tag{25}$$

$$\frac{\partial (\rho \mathbf{v})}{\partial t} + \nabla \cdot (\rho \mathbf{v}\mathbf{v} + p\mathbb{I} + \pi) = (J_\phi \hat{\phi}) \times \mathbf{B} \tag{26}$$

$$J_\phi = \frac{A_\phi}{r^2} - \nabla^2 A_\phi, \tag{27}$$

where $\mathbf{B} = B_r \hat{r} + B_z \hat{z} = \nabla A_\phi \times \nabla \phi$, $\rho\mathbf{v} = \rho v_r \hat{r} + \rho v_z \hat{z}$, D represents kinematic density diffusion, η is resistivity, κ is the anisotropic heat conduction tensor, and π is the viscous tensor. We note that in the absence of $\hat{\phi}$-components of $\mathbf{B}$ and $\mathbf{v}$ in the initial condition, such as in the problem described below, the symmetries of compressible MHD preserve that property throughout a simulation. Thus, we are justified in omitting $\hat{\phi}$-components $\mathbf{B}$ and $\mathbf{v}$ from the above system of PDEs.

A unique feature of this simulation is the use of a scaled coordinate system. The MTF concept involves forming a Field Reversed Configuration (FRC) in a cylindrical flux conserver and then compressing it radially by a factor ~ 10. The most efficient way to model this is to use a grid whose dimensions scale with the motion of the wall. We derive equations that allow us to specify this scaling transformation in the application portion of the code, without requiring any modification of the larger solver portion of the code.

Let $\mathbf{x}$ and $\mathbf{X}$ denote Cartesian representations of the physical and scaled position vectors,

and let $\mathbf{T}(t)$ represent a time-dependent scaling transformation, such that

$$\mathbf{x}(\mathbf{X},t) \equiv \mathbf{T}(t)\cdot\mathbf{X}, \quad \mathbf{X}(\mathbf{x},t) \equiv \mathbf{T}^{-1}(t)\cdot\mathbf{x} \tag{28}$$

To compute the function $u(\mathbf{x}(\mathbf{X},t),t) = u(\mathbf{T}(t)\cdot\mathbf{X},t)$, we use the coordinate transformations

$$\frac{\partial u}{\partial \mathbf{x}}\Big|_t = \frac{\partial}{\partial \mathbf{x}}\mathbf{X}\cdot\frac{\partial u}{\partial \mathbf{X}}\Big|_t = \mathbf{T}^{-1}\cdot\frac{\partial u}{\partial \mathbf{X}}\Big|_t \tag{29}$$

$$\frac{\partial u}{\partial t}\Big|_{\mathbf{x}} = \frac{\partial u}{\partial t}\Big|_{\mathbf{X}} - \mathbf{V}\cdot\frac{\partial u}{\partial \mathbf{x}}, \quad \mathbf{V} \equiv \frac{\partial \mathbf{x}}{\partial t}\Big|_{\mathbf{X}} = \dot{\mathbf{T}}\cdot\mathbf{X} \tag{30}$$

with $\dot{\mathbf{T}} \equiv d\mathbf{T}/dt$. A general system of flux-source equations in physical coordinates of the form

$$A\frac{\partial u}{\partial t}\Big|_{\mathbf{x}} + \frac{\partial}{\partial \mathbf{x}}\cdot\mathbf{F}\Big|_t = S \tag{31}$$

is then equivalent to the equation in scaled coordinates of the form

$$A\frac{\partial u}{\partial t}\Big|_{\mathbf{X}} + \frac{\partial}{\partial \mathbf{X}}\cdot\mathbf{F}'\Big|_t = S' \tag{32}$$

with

$$\mathbf{F}' \equiv \mathbf{F}\cdot\mathbf{T}^{-1}, \quad S' = S + A\left(\dot{\mathbf{T}}\cdot\mathbf{X}\right)\cdot\left(\mathbf{T}^{-1}\cdot\frac{\partial u}{\partial \mathbf{X}}\right) \tag{33}$$

In the MTF radial compression problem, we define $\mathbf{T}(t)$ to represent the moving radial wall $r = T(t)R$, with $T(t) = a\cos(\omega t)+b$, $a = (T_{init}-T_{final})/2$, $b = (T_{init}+T_{final})/2$, $\omega = \pi/t_{stag}$, with the scaled coordinate $R \in [0,1]$. Figs. 3-4 show results of a simulation with $T_{init} = 1$, $T_{final} = 0.1$, and $t_{stag} = 100$.

The initial conditions in the simulation use a numerical solution of the Grad-Shafranov equation with the vector potential A_ϕ shown in panel (a) of Figure 3, plasma density $\rho \propto p^{1/2}$, and no plasma flow. The initial plasma pressure p outside of the FRC magnetic separatrix is set to be uniform at 0.3% of the peak initial pressure at the center of the FRC. Perfectly-conducting, impenetrable, non-slip, thermally insulating boundary conditions have been imposed at the moving radial wall, and the system is assumed to be periodic in the axial $\hat{z}$-direction.

The resulting final magnetic configuration at $t = t_{stag}$ after radial compression by $T_{init}/T_{final} = 10$ is shown in panel (b) of Figure 3. Note that in addition to radial com-

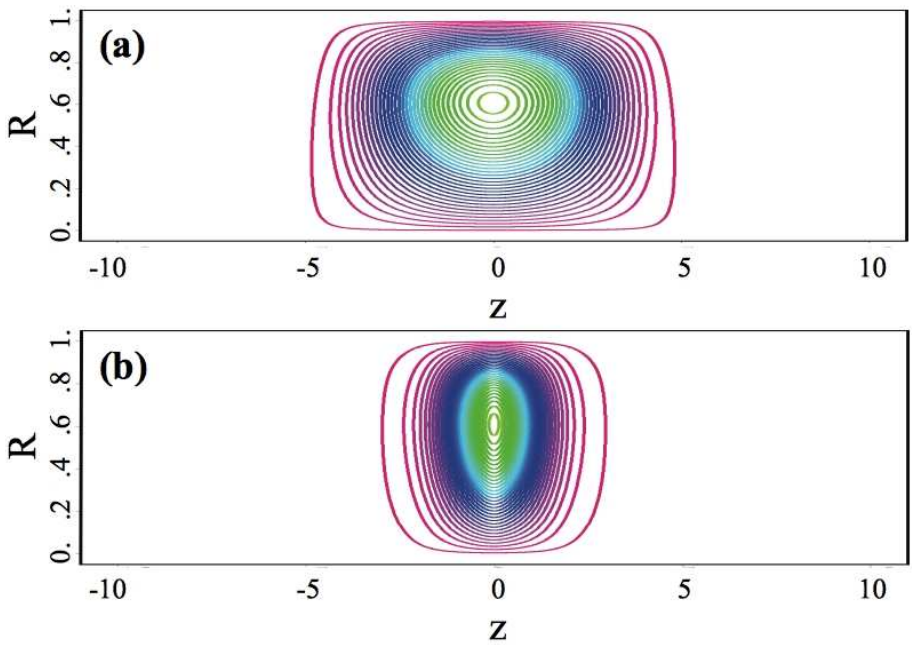

FIG. 3: Contour plot of magnetic vector potential A_ϕ *vs.* scaled radial variable R and physical axial variable z before [panel (a)] and after [panel (b)] radial compression by a factor of 10. Note that the FRC experiences axial as well as radial compression due to magnetic tension.

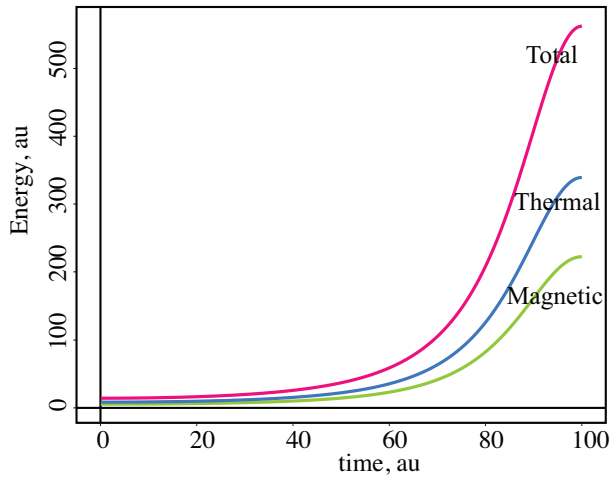

FIG. 4: Volume integrals of total, thermal, and magnetic energy *vs.* time t during the radial compression.

pression, the FRC also experiences axial compression due to magnetic tension. Figure 4 shows time-traces of total, thermal and magnetic energy in the system throughout the simulation. The force acting to compress the flux-conserver against the thermal and magnetic back-pressure of the FRC provides the energy source in the system. It is clear that most of the energy input goes into the thermal energy, demonstrating the promise of the MTF

method for fusion applications.

C. 3D compressible Hall MHD spheromak tilt study

An example of 3D HiFi application is a compressible Hall MHD study of the non-linear dynamics of a tilting spheromak, conducted on a cylindrical grid solving the following set of normalized PDEs expressed in the Cartesian coordinate system:

$$\frac{\partial \rho}{\partial t} + \nabla \cdot (\rho \mathbf{v}_i) = 0 \tag{34}$$

$$\frac{\partial (\rho \mathbf{v}_i)}{\partial t} + \nabla \cdot [\rho \mathbf{v}_i \mathbf{v}_i + p\mathbb{I} - \bar{\mu}\nabla \mathbf{v}_i - \bar{\nu}\nabla \mathbf{v}_e] = \mathbf{J} \times \mathbf{B} \tag{35}$$

$$\frac{\partial \mathbf{A}}{\partial t} = \mathbf{v}_e \times \mathbf{B} + \frac{d_i}{\rho}\nabla p_e - \bar{\eta}\mathbf{J} - \frac{d_i}{\rho}\bar{\nu}\nabla^2 \mathbf{v}_e \tag{36}$$

$$\nabla \cdot [(\nabla \cdot \mathbf{A})\mathbb{I} - \nabla \mathbf{A}] = \mathbf{J} \tag{37}$$

$$\frac{3}{2}\frac{\partial p}{\partial t} + \nabla \cdot \left[\frac{5}{2}(p_i \mathbf{v}_i + p_e \mathbf{v}_e) - \bar{\kappa}\nabla T\right] = \mathbf{v}_i \cdot \nabla p_i + \mathbf{v}_e \cdot \nabla p_e + \bar{\eta}|\mathbf{J}|^2 + \bar{\mu}\nabla \mathbf{v}_i : \nabla \mathbf{v}_i + \bar{\nu}\nabla \mathbf{v}_e : \nabla \mathbf{v}_e \tag{38}$$

where $\mathbf{B} = \nabla \times \mathbf{A}$, $\mathbf{v}_e = (\rho \mathbf{v}_i - d_i \mathbf{J})/\rho$, $p = \rho T = p_i + p_e$, $p_e/p_i = \alpha = const$, $d_i = (c/\omega_{pi})/L_0 = (c/L_0 e)\sqrt{m_i/4\pi n_0}$, $\bar{\eta} = (\eta c^2/L_0 B_0)\sqrt{m_i n_0/4\pi}$, $\bar{\mu} = (\mu_i/L_0 B_0)\sqrt{4\pi/m_i n_0}$, $\bar{\nu} = (\mu_e/L_0 B_0)\sqrt{4\pi/m_i n_0}$, $\bar{\kappa} = (\kappa/L_0 B_0)\sqrt{4\pi m_i/n_0}$, and $\{\eta, \mu_i, \mu_e, \kappa\}$ are some physical values for resistivity, ion viscosity, electron viscosity and heat conduction (assumed to be isotropic with $\kappa = \kappa_e = \kappa_i$), respectively. Note that all normalizations are determined by the choices for L_0, B_0, and n_0.

The computational domain is a cylinder of radius $R = L_0$ and length $L = 2L_0$, with the cylindrical BC applied at the cylindrical axis. The simulation is initialized with a stationary axisymmetric Solov'ev spheromak equilibrium with uniform normalized pressure and density of $p = \rho = 1$, and $O(10^{-2})$ tilting perturbation in axial ion velocity v_{iz}. The following perfect conductor ($\hat{n} \times (\partial \mathbf{A}/\partial t) = \mathbf{0}$) non-penetrable ($\hat{n} \cdot \mathbf{v}_i = 0$) energy-conserving BC are imposed: heat insulator $\hat{n} \cdot \nabla T = 0$, perfect slip ion flow $\hat{n} \cdot \nabla(\hat{n} \times \mathbf{v}) = \mathbf{0}$, perfect slip electron flow $\hat{n} \cdot \nabla \mathbf{v}_e = \mathbf{0}$. Additionally, $\nabla \cdot \mathbf{A} = 0$ is imposed to specify the electro-magnetic gauge BC.

The simulation data shown in Figure 5 was obtained with the following values for the

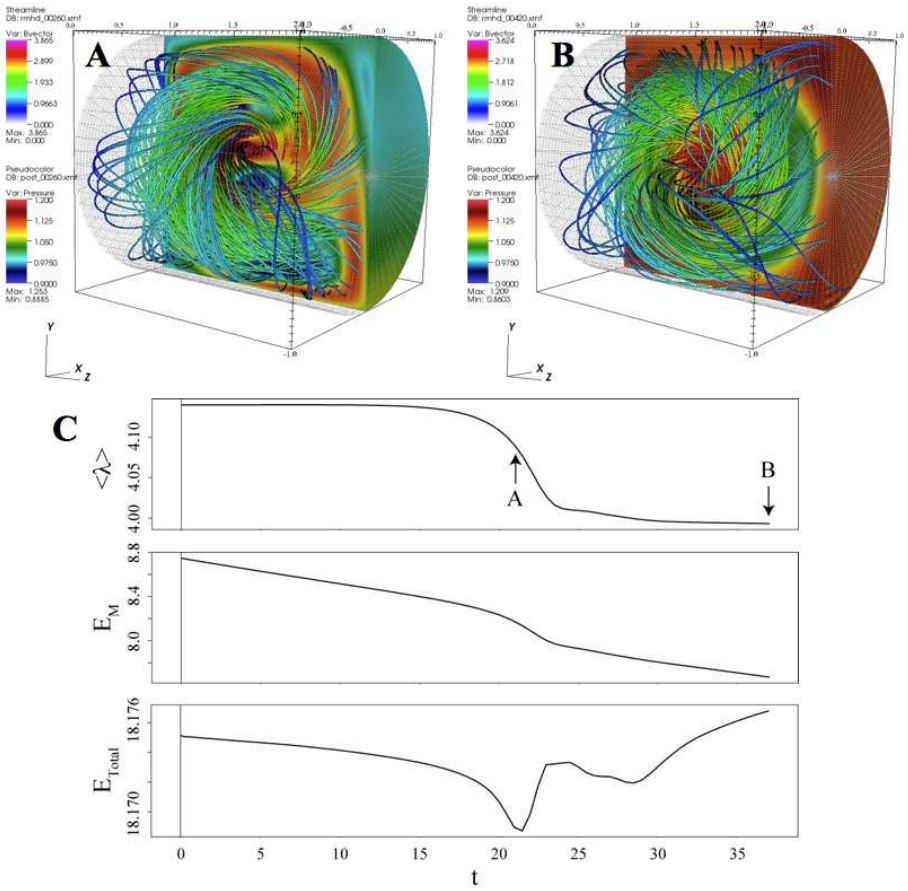

FIG. 5: Frames A and B show magnetic field lines (streamlines color-coded by $|\mathbf{B}|$) and plasma pressure (pseudocolor cutaway) at two different times during a Hall MHD spheromak tilt simulation. The time-stamps of frames A and B are shown in frame C, where the evolution of $< \lambda > \equiv 2E_M/K$ (ratio of magnetic energy to magnetic helicity), magnetic energy E_M, and total energy E_{Total} are shown throughout the simulation.

dimensionless parameters in the PDE system specified above: $\alpha = 0$, $d_i = 10^{-1}$, $\bar{\eta} = 0$, $\bar{\mu} = 10^{-2}$, $\bar{\nu} = 5 \times 10^{-4}$ and $\bar{\kappa} = 10^{-1}$. A computational grid of $(n_r, n_\phi, n_z, n_p) = (6, 6, 6, 5)$ was used with the grid distributed uniformly in the radial, angular, and axial directions.

Frames A and B of Figure 5 show streamlines of magnetic field color-coded by $|\mathbf{B}|$ and pseudocolor cutaway of plasma pressure p in the midst of the tilting (frame A) and fully relaxed (frame B). The time-stamps of frames A and B are shown in frame C, where the the top panel shows the evolution of $< \lambda > \equiv 2E_M/K$, where $E_M \equiv 1/2 \int \mathbf{B} \cdot \mathbf{B}\, dV$ is the magnetic energy and $K \equiv \int \mathbf{A} \cdot \mathbf{B}\, dV$ is the magnetic helicity in the system.

We note that in closed systems with low magnetic dissipation, such as the one considered here, magnetic field is thought to relax to the lowest available energy state, while its helicity

remains approximately constant[38, 39]. Such relaxed Woltjer-Taylor states must satisfy

$$\nabla \times \mathbf{B} = \lambda \mathbf{B}, \tag{39}$$

where λ is a constant. It is easy to show that in a closed system where magnetic field satisfies Eq. (39), $< \lambda >= \lambda$. In fact, the initial axisymmetric spheromak state of the simulation can be described by $\lambda = 4.138/L_0$, while the lowest energy Woltjer-Taylor state in the perfectly-conducting $L : R = 2 : 1$ cylinder has $\lambda = 3.978/L_0$ – and top panel of frame C in Fig. 5 shows normalized $< \lambda >$ dropping from 4.138 to 3.978 as the magnetic fields relax.

The bottom two panels of Fig. 5 show the magnetic energy E_M and the total energy E_{Total} versus time throughout the simulation. We observe that, as expected, the steady loss of magnetic energy due to the electron viscous term in Eq. (36) is accelerated when the spheromak begins to tilt, and then settles down to a slower rate of decay as the system approaches the relaxed state. We measure the total energy of the system to be conserved to about 5 parts in 10^4. It should be emphasized that we do not evolve total energy as one of the dependent variables nor use any special techniques designed to conserve energy in the simulation; the energy conservation is due purely to solving PDEs with boundary conditions that analytically conserve energy in the continuous limit.

VIII. SUMMARY AND FUTURE DEVELOPMENT PLANS

In this manuscript, we have described the HiFi implicit high order finite (spectral) element modeling framework for multi-fluid plasma applications. The general flux-source form of the PDEs required by HiFi, the details of the spatial and temporal discretization, the boundary condition options, as well as the user interface and several additional features of the framework have been presented. Several recent applications of the framework to presently-relevant research problems spanning the range from simple 2D to complex 3D systems of PDEs have been described.

In addition to the presently available capabilities and flexibilities of the HiFi framework, several development efforts to enhance and expand the framework's ability to model various idealized, experimental and naturally occurring physical systems are ongoing or being planned for the near future.

Implementation of the generalized PBP method to precondition the linear systems resulting from the implicit advance of PDEs spatially discretized in the weak form using the spectral element basis set is one of the ongoing development efforts. When completed, it is projected that PBP will allow HiFi to scale to tens of thousands of processors and beyond. Furthermore, it will at least halve the amount of memory presently required to run a given HiFi simulation.

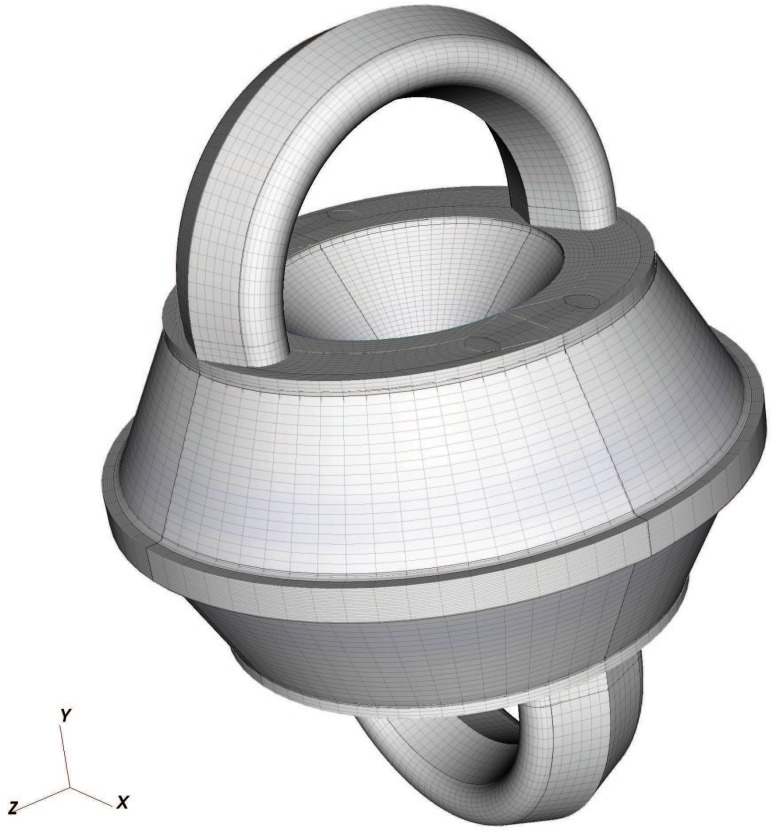

FIG. 6: Multi-block computational grid for a planned extended MHD simulation of a HIT-SI experiment[11].

Another significant and very recent addition to the HiFi toolbox is the semi-structured grid capability. Figure 6 shows an example of the computational grid composed of several structured grid blocks that has been successfully used for preliminary testing using the 3D anisotropic heat conduction equation and the 3D MHD system of PDEs[11]. The goal of this development effort has been to enable HiFi simulations on computational grids of arbitrary three-dimensional geometry and topology. In the future, this may include the ability to use

spectral elements of different n_p order in the different parts of the computational domain, as well as n_p-adaptation.

HiFi is an open-source development project and has been released under a BSD-style license. Latest verified versions of the framework are available to the greater scientific research community upon request.

Acknowledgements

This work was supported, in part, by the U.S. Department of Energy and the Office of Naval Research. To date, HiFi development has taken place, in chronological order, at the following institutions: Los Alamos National Laboratory, Princeton Plasma Physics Laboratory, University of Washington, and U.S. Naval Research Laboratory. We gratefully acknowledge helpful discussions with and occasional coding contributions from L. Chacòn, S.C. Jardin, M. Sato, U. Shumlak, A.N. Simakov, C.R. Sovinec and X.Z. Tang.

---

[1] W.-C. Müller and D. Biskamp, Phys. Rev. Lett. **84**, 475 (2000).

[2] J. C. Perez and S. Boldyrev, Phys. Rev. Lett. **102**, 025003 (2009).

[3] C. R. Sovinec, A. H. Glasser, T. A. Gianakon, D. C. Barnes, R. A. Nebel, S. E. Kruger, D. D. Schnack, S. J. Plimpton, A. Tarditi, and the NIMROD Team, J. Comput. Phys. **195**, 355 (2004).

[4] *Comsol multiphysics*, URL `http://www.comsol.com/`.

[5] A. H. Glasser and X. Z. Tang, Comp. Phys. Comm. **164**, 237 (2004).

[6] G. E. Karniadakis and S. J. Sherwin, *Spectral/hp Element Methods for CFD* (Oxford University Press, New York, 1999).

[7] M. O. DEVILLE, P. F. FISCHER, and E. H. MUND, *High-Order Methods for Incompressible Fluid Flow* (Cambridge University Press, 2002).

[8] *Portable, extensible toolkit for scientific computation (PETSc)*, URL `http://www.mcs.anl.gov/petsc`.

[9] V. S. Lukin, Ph.D. thesis, Princeton University (2008).

[10] E. T. Meier, Ph.D. thesis, University of Washington (2011).

[11] W. B. Lowrie, Ph.D. thesis, University of Washington (2011).

[12] S. C. Jardin and J. A. Breslau, Phys. Plasmas **12**, 56101 (2005).

[13] R. E. Bank, W. M. Coughran, W. Fichtner, E. H. Grosse, D. J. Rose, and R. K. Smith, IEEE Transactions on Electron Devices **32**, 1992 (1985).

[14] L. Chacòn, Phys. Plasmas **15**, 056103 (2008).

[15] M. Berger and J. Oliger, J. Comput. Phys. **53**, 484 (1984).

[16] M. J. Berger and P. Collela, J. Comput. Phys. **82**, 64 (1989).

[17] C. W. Hirt, A. A. Amsden, and J. L. Cook, J. Comput. Phys. **14**, 227 (1974).

[18] S. C. Jardin, J. L. Johnson, J. M. Greene, and R. C. Grimm, J. Comp. Phys. **29**, 101 (1978).

[19] D. S. Kershaw, M. K. Prasad, M. J. Shaw, and J. L. Milovich, Comput. Methods Appl. Engrg. **158**, 81 (1998).

[20] J. U. Brackbill and H. M. Ruppel, J. Comput. Phys. **65**, 314 (1986).

[21] J. U. Brackbill, J. Comput. Phys. **108**, 38 (1993).

[22] P. Knupp, J. Comput. Phys. **119**, 142 (1995).

[23] R. W. Anderson, N. S. Elliott, and R. B. Pember, J. Comput. Phys. **199**, 598 (2004).

[24] V. D. Liseikin, *A Computational Differential Geometry Approach to Grid Generation* (Springer Verlag, 2003).

[25] *The HDF group*, URL `http://www.hdfgroup.org/HDF5/`.

[26] *VisIt Visualization Tool*, URL `http://wci.llnl.gov/codes/visit/`.

[27] V. S. Lukin, Phys. Plasmas **16**, 122105 (2009).

[28] V. S. Lukin and M. G. Linton, Nonlin. Processes Geophys. **18**, 871 (2011).

[29] T. Gray, V. S. Lukin, M. R. Brown, and C. D. Cothran, Phys. Plasmas **17**, 102106 (2010).

[30] C. D. Cothran, M. R. Brown, T. Gray, M. J. Schaffer, G. Marklin, and V. S. Lukin, Phys. Plasmas **17**, 055705 (2010).

[31] E. T. Meier, V. S. Lukin, and U. Shumlak, Comp. Phys. Comm. **181**, 837 (2010).

[32] W. Lowrie, V. S. Lukin, and U. Shumlak, J. Comput. Phys. **230**, 5564 (2011).

[33] E. T. Meier, A. H. Glasser, V. S. Lukin, and U. Shumlak, J. Comput. Phys. **231**, 2963 (2012).

[34] E. G. Harris, Nuovo Cimento **23**, 115 (1962).

[35] N. F. Loureiro, A. A. Schekochihin, and S. C. Cowley, Phys. Plasmas **14**, 100703 (2007).

[36] G. A. Wurden, K. F. Schoenberg, R. E. Siemon, M. Tuszewski, F. J. Wysocki, and R. D. Milroy, in *Proceedings of the 9th International Toki Conference on Plasma Physics and Controlled*

Nuclear Fusion (Toki, Japan, 1998), p. 238.

[37] J. M. Taccetti, T. P. Intrator, G. A. Wurden, S. Y. Zhang, R. Aragonez, P. N. Assmus, C. M. Bass, C. Carey, S. A. deVries, W. J. Fienup, et al., Rev. Sci. Instr. **74**, 4314 (2003).

[38] L. Woltjer, Proc. Nat. Acad. Sci. **44**, 489 (1958).

[39] J. B. Taylor, Phys. Rev. Lett. **33**, 1139 (1974).